# High Power Density DC-DC Converter with SiC MOSFETs for Electric Vehicles

*G. Calderon-Lopez, A. J. Forsyth*

*Power Conversion Group, School of Electrical and Electronic Engineering, University of Manchester, UK,*
*gerardo.calderon-lopez@manchester.ac.uk, andrew.forsyth@manchester.ac.uk*

**Keywords:** DC-DC converter, bi-directional interleaved, inter-phase transformer, power-dense, electric vehicle.

## Abstract

This paper shows the performance evaluation and practical demonstration of a high-power bi-directional DC-DC converter with a power density of 20 kW/l, using 1200V/100A SiC MOSFET modules from CREE. The converter is based on a dual-interleaved topology with hard-switching operating at 75 kHz. To increase the power density, water-cooled magnetic components are used. The experimental results of a 60 kW converter show the potential to increase the operating frequencies up to 100 kHz and beyond in this application.

## 1 Introduction

For high blocking voltages, silicon (Si) MOSFETs have the drawback of having larger on-state resistances leading to higher conduction losses at high current levels; therefore, the use of Si MOSFETs in high voltage, high current applications has been limited, making the Si IGBT the preferred device.

Nowadays, the use of silicon carbide (SiC) devices such as BJTs, MOSFETs and Schottky diodes is expanding rapidly as they overcome many drawbacks of silicon devices [1, 2]. In the last few years, several SiC devices have become commercially-available and even though their price is higher than Si parts with similar ratings, they offer lower on-state and switching losses, the capability to switch at higher frequencies, and have reduced cooling requirements, making them attractive for highly demanding applications, such as on-board an electric vehicle or in a more-electric aircraft.

The traction system on board an electric vehicle typically operates at 600 V to reduce losses, whilst battery packs tend to be rated around 300 V, therefore a bi-directional DC-DC converter is required between the two. Since the converter must be rated to carry the full traction power it can be a large and heavy item, with the magnetic components accounting for between a third and a half of the total weight. Therefore, one of the ways to reduce the overall converter size is to increase the switching frequency, which usually leads to smaller magnetic components. The superior characteristics of SiC power devices provide the possibility to increase converter operating frequencies without degrading system efficiency and this forms the basis of the current work.

This paper deals with the design and performance evaluation of a 600 V, 60 kW bi-directional DC-DC converter operating at 75 kHz, and using 1200V/100A SiC MOSFET modules available now on the market. First, the system topology and the schematic of the converter are presented; here, the SiC power modules and the selection of the switching frequency are provided along with the characteristics of the magnetic components. Then relevant construction details of the cooling system, bus bars and gate drivers are given. Finally, the performance evaluation of the converter operating at different conditions is reported.

## 2 System topology and circuit

The SiC DC-DC converter forms part of a three-port converter to interface a low voltage supercapacitor bank, a lithium battery and the traction drive in an electric vehicle. Each port is interfaced with an individual dual interleaved, bi-directional converter with inter-phase transformer (IPT). This independent structure allows the optimisation of the switching frequencies of each converter to minimise the weight of the magnetic components, achieving high power density and maximising the efficiency of the overall unit.

Fig. 1 shows the schematic of the dual-interleaved bi-directional converter with IPT, a well-known topology for electric vehicles with reduced number of components, simple PWM control and high efficiency [3-7].

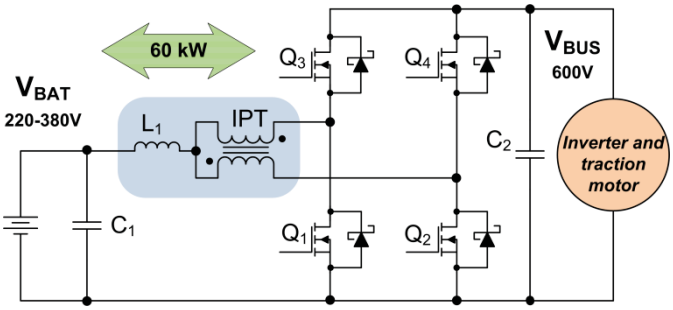


Fig. 1. Dual interleaved bidirectional converter with IPT.

### 2.1 SiC power modules

CREE 1200V/100A power modules were selected, part number CAS100H12AM1 [8], featuring a half-bridge of SiC MOSFETs with anti-parallel Schottky diodes, low switching losses and 16-mΩ on-state resistance at 25 °C. Assuming that the total input current is perfectly shared between both

phases, the conduction and switching losses for MOSFETs and diodes are calculated under the worst-operating conditions and maximum power throughput. Then, the temperature rise on the junctions of the dies is estimated by using the thermal conductivities provided on the datasheet. The converter was designed to operate with a maximum cold plate temperature of 60 °C and a maximum junction temperature of 150 °C.

### 2.2 Selection of switching frequency

Fig. 2 shows the ideal maximum allowable power transfer of the converter considering a junction temperature of 150 °C in the MOSFETs. The switching frequency varies in the range 50 kHz-150 kHz, and three conditions of $V_{BAT}$ are shown: 220 V, 300 V and 380 V.

As the switching frequency increases, the maximum power throughput reduces due to higher switching losses. At 60 kW and 380 V, this plot suggests that a maximum switching frequency above 120 kHz is feasible. However, as the voltage in the battery reduces, the maximum power also decreases because of higher battery currents.

An operating frequency of 75 kHz was selected as a compromise between making a significant reduction in magnetic weight compared with a Si IGBT system whilst still being able to achieve a power throughput of 40 kW at the lower extreme of the battery voltage.

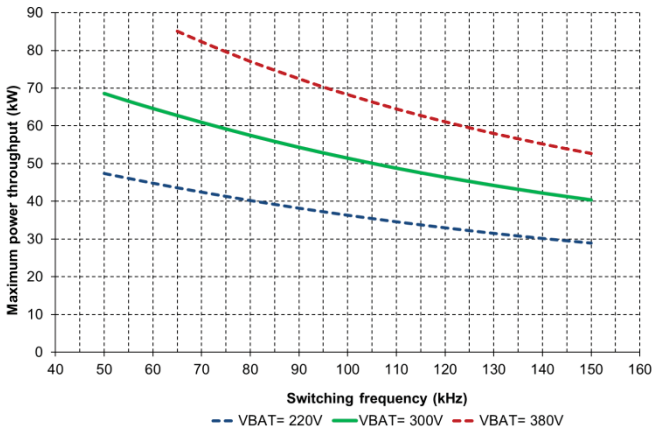


Fig. 2. Ideal maximum power throughput at different switching frequencies, $V_{BUS}$= 600 V, $T_j$= 150 °C.

### 2.3 Magnetic components

The inductor and the IPT use nano-crystalline amorphous metal cores from Hitachi Metals, Finemet, due to its high saturation point (1.23 T), low core losses, and high operating temperature (155 °C) [9]. The inductor is designed to handle the high DC current (up to 260 A) plus the AC ripple current resulting from the worst-operating conditions at twice the switching frequency, whilst the IPT is designed to operate at the switching frequency with maximum output voltage and 50 % duty ratio.

Conduction cooling to the converter cold plate is used to increase the current density in the magnetic components, minimise the size & volume, and remove the heat from the cores and windings efficiently. Therefore, both devices are potted into a single aluminium can which is bolted to the main cold plate. For potting, a high thermal conductivity epoxy resin is used, and the whole unit is degassed before curing to remove any air bubbles which might impair the thermal transfer. Finite-element simulations were used to identify the hot-spot temperatures in the cores, and keep them below the 155 °C limit. Fig. 3 shows a 3D drawing of the potted magnetic components.

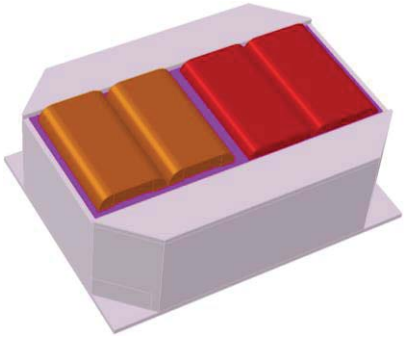

Fig. 3. 3D-model of the potted magnetic components for thermal FEA.

## 3 Construction details

Fig. 4 presents an exploded view of the main parts of the converter. Copper studs were used to connect the terminals from the IPT to their corresponding pads on the SiC power modules, and to measure the winding currents with the transducers. To ensure the current sharing between the phases, a peak current mode controller is used to generate the PWM signals for the switches.

### 3.1 Water-cooled heat sinks

Using 3D CAD software, the main components of the converter were modelled and then a suitable off-the-shelf cold plate was identified for the best possible layout with the shortest connections between the planar bus bars, magnetic components and power modules. The cold plate is formed by two CP12G06 from Lytron, arranged in a side-by-side configuration. These are 4-pass copper tubed Al cold plates with dimensions 305 × 152 × 13 mm, dual-side mounting, and low pressure drop [10]. According to the datasheet, the estimated thermal resistances of the cold plate at 7.57 litres per minute are 0.009°C/W on the tube side and 0.013°C/W on the plate side.

The pipes in the middle of the cold plates are coupled with elbows and copper tube of the same diameter. An aluminium tray underneath the cold plates is used to frame and hold them, providing a robust mechanical support. All the devices are mounted on the tube side for the best thermal performance. The water inlet and outlet have adapters for 16-mm inner diameter hose, and the cooling system has a water pump with a measured water flow of 9 litres per minute.

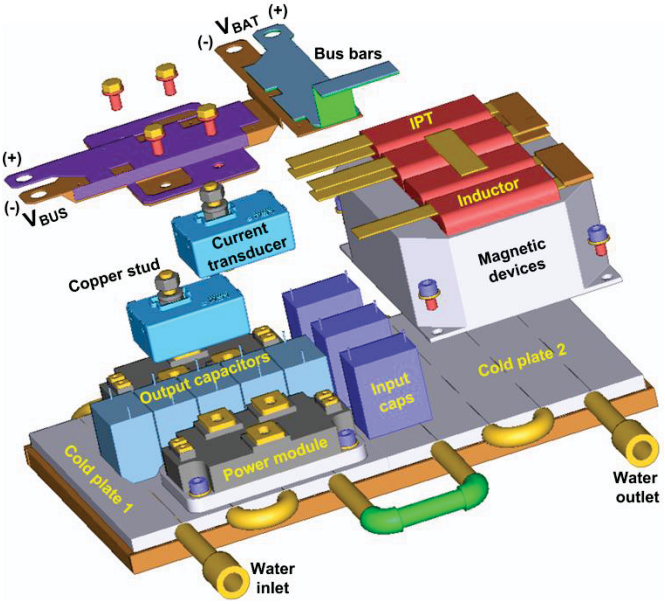


Fig. 4. Assembly of the SiC converter.

### 3.2 Bus bars and filter capacitors

Planar copper bus bars were used to keep the parasitic inductances as low as possible. Each bus bar is insulated with a thin layer of adhesive Kapton film, and the input and output capacitors are directly soldered to the bus bars. To use the available space to the maximum extent, a folded bus bar was designed to cope with the different heights between the capacitors, power modules and magnetic components.

Power film capacitors with polypropylene dielectric are used for DC filtering, three metallised polypropylene capacitors (MKP) from EPCOS (5 µF, 630 V) in the input capacitor bank, and five medium power film capacitors from AVX (7.5 µF, 720 V) for the output capacitor.

The terminals for the battery and traction drive ports form part of the bus bars, and M8 brass bolts and washers are used for the connections to the source/load.

### 3.3 Weight and volume

Table 1 presents a detailed breakdown of components' weights in the converter, and Fig. 5 shows a pie chart to identify the contributions of each part to the overall weight, that is, 5.2 kg. Assuming a continuous operation from 380 V to 600 V and 60 kW, the gravimetric power density is 11.5 kW/kg. The approximate dimensions of the box around the converter are 254 ×152 × 77 mm, that is, a volume slightly less than 3 litres, meaning a volumetric power density of 20 kW/l. It is interesting to note that almost 80 % of the total weight corresponds to the magnetic components and cooling means; however, the latter could be reduced further if a bespoke, high performance cooling technique is used.

### 3.4 Gate drivers

The converter uses two off-the-shelf gate drivers from CONCEPT, part number 2SC0650P2A0-17. These are dual-channel drivers featuring high power (6 W per channel), high frequency capability up to 150 kHz, and a low profile of only 6.5 mm [11]. Their flat design achieved with planar transformer technology allowed double-side mounting onto a main PCB with the required auxiliary components for protection, filtering and gate resistors, whilst keeping an overall low profile.

Finally, Fig. 6 shows a picture of the converter including the gate drivers.

| *Component* | *Weight (kg)* |
|---|---|
| Magnetic devices | 2.5 |
| Cold plates | 1.6 |
| Power modules and gate drivers | 0.4 |
| Mounting and cooling hardware | 0.3 |
| Control and busbars | 0.2 |
| Input & output capacitors | 0.2 |
| TOTAL | 5.2 |

Table 1: Weight of the SiC converter's components.

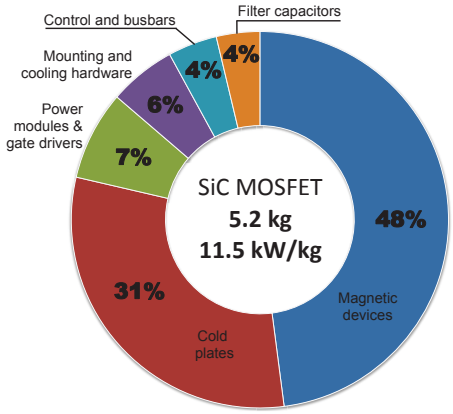


Fig. 5. Breakdown of weights in the SiC converter.

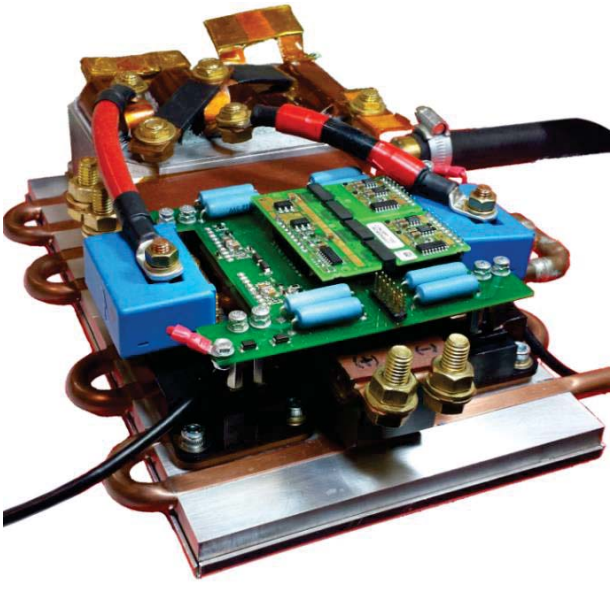

Fig. 6. Picture of the SiC converter.

As can be seen in Fig. 6, the main PCB for gate driving was designed to rest on the top of the bus bars and fit into the space between the current transducers, the input capacitor bank and the terminals of the high voltage port, $V_{BUS}$. To achieve short connections to the gate terminals on the power modules, their corresponding pads on the main driving board were located just above their approximated positions, and 22mm-height M2 pillars were used for interconnection. The dimensions of the gate driver board are 132 × 98 × 23 mm.

Two 5 W, 3 Ω resistors are used per switch since the drivers use independent gate resistors for turn-on and turn-off. They also feature a dedicated MOSFET mode; however, this mode only features a turn-off voltage of 0 V [12], and the recommended gate voltages for driving the SiC MOSFETs by CREE are +20 V/–5 V. Therefore, the suggested circuit for this mode from the application note [12] was modified by adding a negative reference to the source terminals with the aid of 5.1-V Zener diodes. The measured gate voltages on the drivers are +19.6 V for turn-on and −5.5 V at turn-off, with peak currents of ± 2.5 A.

## 4 Performance evaluation

The converter was successfully tested at the minimum and maximum input voltages, 220 V and 380 V, in boost mode to 600 V, at 41 kW and 60 kW power throughputs, respectively. For each voltage condition several steps of power levels were tested before reaching the maximum, and their efficiencies were measured, along with the drain-to-source voltages and the drain currents flowing in the MOSFETs. Temperature sensors were located on the case of the power modules and on the cold plate to obtain their temperature rise, and ensure that the converter reached its steady-state thermal condition.

Measured and estimated figures of efficiencies were compared for each operating point, and they showed a good correlation. The estimated efficiencies were derived with estimations of power losses from the semiconductors (switching and conduction losses) and from the magnetic components (core, gap and copper losses). Furthermore, the measured temperatures in the case and cold plate also showed a good agreement with expected values using the calculated power losses and the component's thermal resistances.

### 4.1 Performance during switching

Fig. 7a shows the turn-on transient in one of the phases of the converter operating from 380 V to 600 V, at 60.3 kW, whereas Fig. 7b depicts the turn-off transient. From top to bottom, the waveforms show the measured drain-to-source voltage, $V_{DS}$, drain current, $I_D$, and their instantaneous transient power, $p_{ON}$ and $p_{OFF}$. From the current waveform at turn-on, it is clear that there are virtually zero reverse-recovery losses due to the ultra-fast operation of the Schottky diodes. The approximated peak reverse-recovery current is about 60 A, with a reverse-recovery time close to 35 ns. From the power plots, it can be seen that the turn-off transient dissipates more energy than the turn-on instant. Table 2 summarises the switching performance of the converter. The energy losses per switching transient were measured by integrating the corresponding instantaneous power plot. The total energy losses are only 2.16 mJ, giving a total switching loss of 162 W at 75 kHz. The calculated figure at this operating condition is 170 W, using interpolation from datasheet values.

The measured *di/dt* exceeds 2 kA/μs, and the voltage overshoot at turn-off is 145 V indicating a stray inductance close to 70 nH.

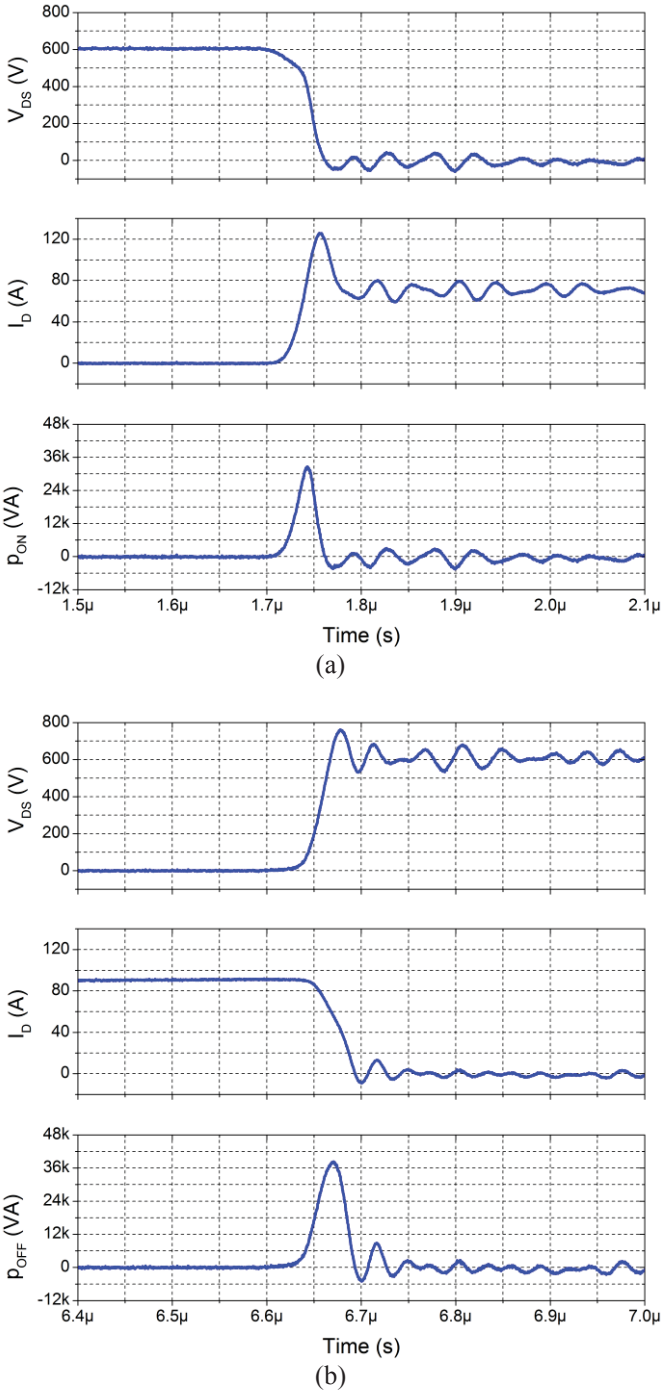


Fig. 7. Turn-on and turn-off switching transients in the SiC converter, 380 V - 600 V, 60.3 kW, 74.6 kHz, 50 ns/div.

| *Transient* | *Performance indicator* | | *Value* |
|---|---|---|---|
| Turn-on | Voltage fall time | (ns) | 35 |
| | Current rise time | (ns) | 20 |
| | Energy losses | (mJ) | 0.8 |
| Turn-off | Voltage rise time | (ns) | 25 |
| | Current fall time | (ns) | 37 |
| | Energy losses | (mJ) | 1.36 |
| | Total switching losses | (mJ) | 2.16 |

Table 2: Measured performance indicators during hard-switching conditions, 380 V - 600 V, 60.3 kW.

### 4.2 Performance during conduction

The resistances from drain to source of the bottom MOSFETs in both power modules were measured by using a constant current source and measuring its voltage drop with a high precision, 6.5-digit multimeter (model 34401A from Agilent), whilst keeping on their respective gates. Several steps of current were measured from 3 A to 100 A, and at least 4 different measurements were taken per switch. Fig. 8 presents the averaged values of the $R_{DS(on)}$ at room temperature for each power module. It can be seen that the module on the right of Fig. 6 has approximately 0.75 mΩ more resistance than the left one; meanwhile both increase with almost the same slope with the drain current. At 100 A, the resistances are above the typical value of 16 mΩ, but lie within the 25 % tolerance stated in the datasheet. The positive slope in $R_{DS(on)}$ with the increment of $I_D$ is steeper than that in the datasheet, but this could be caused by the increase in $T_j$ during the measurement. For calculating the power losses during the conduction periods, a linear interpolation was used to approximate the value of the $R_{DS(on)}$. The equation is,

$$R_{DS(on)} = 14.8 + 0.028\, I_D \quad [m\Omega] \qquad (1)$$

To determine the increment of the drain-to-source resistance with the temperature, the plot of the normalised resistance vs junction temperature from the datasheet (Fig. 4 on Ref. [8]) was used. According to the cited plot at $T_j$= 125 °C, the resistance increases by almost 20 %.

Then, the conduction losses due to the switches at different operating conditions were estimated by using Equation (1), the normalised value at 125 °C, and the square of the RMS current flowing through the switches.

Concerning the conduction losses of the diodes during the free-wheeling periods, the equivalent forward voltage was calculated by interpolating the corresponding plot from the datasheet (Fig. 12 on [8]) for the average diode's current with $V_{GS}$= −5 V and a $T_j$= 150 °C. The 5-th order polynomial interpolation employed for these calculations is,

$$V_{DS} = -3.2\times10^{-11} I_D^5 + 1.82\times10^{-8} I_D^4 - 3.4\times10^{-6} I_D^3 + 1.55\times10^{-4} I_D^2 + 2.37\times10^{-2} I_D + 0.72 \quad [V] \qquad (2)$$

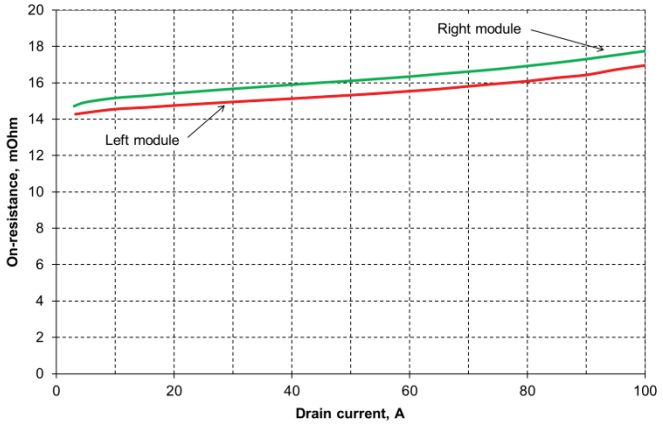


Fig. 8. Measured on-state resistances of the lower MOSFETs at room temperature.

### 4.3 Efficiency measurements

The efficiencies were measured by monitoring the input and output voltages with two high precision meters 34401A, and the averaged values of input and output currents were obtained with the oscilloscope and high current LeCroy probes, CP500 and CP150, respectively, over a period of at least 100 ms. At 380 V to 600 V, 60.4 kW, a minimum efficiency of 98.7 % was obtained, meaning an overall power loss close to 790 W. The approximated efficiency using the calculations of power losses in semiconductor and magnetic devices is 98.6 %, that is a total power loss of 830 W.

Concerning the operation at minimum input voltage and 41 kW, the measured efficiency is 97.5 %, that is, a loss of 1040 W. Comparatively, the estimations are 97.4 % and total losses of 1055 W.

### 4.4 Thermal measurements

Fig. 9 shows the average temperatures measured in the case, cold plate and ambient of the power modules when operating from 220 V to 600 V, and 40.6 kW. The total time of the test was over 50 minutes, and the temperatures were recorded once every second. The steady-state operation was achieved after 30 minutes. By using the thermal resistances from the datasheets of the modules and cold plate, for the stated operating conditions with an ambient temperature of 34 °C, the predicted temperatures of the cold plate are 42°C, on the cases of the power modules 52 °C, on the junction of the switches 131 °C, and on the junction of the diodes 85 °C. As can be confirmed by the plot, the temperatures of the cold plate near the power modules are below 45 °C, whilst the cases are close to 51 °C. Therefore, a good agreement between measured and predicted temperatures has been achieved.

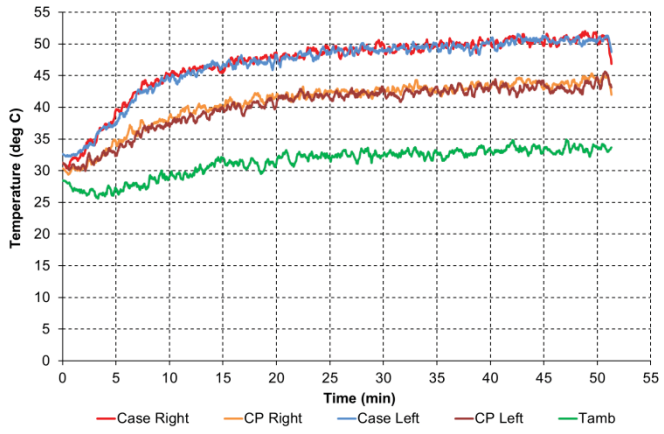


Fig. 9. Measured temperatures in the power modules and cold plate (CP), $V_{BAT}$= 220 V, $V_{BUS}$= 600 V, P= 40.6 kW.

## 5 Conclusions

This paper has presented a high power DC-DC converter with silicon carbide power modules readily available on the market. Features of the magnetic components, cooling system, bus bars and filter capacitors used in the prototype have been provided, and experimental results were shown to verify the design. It has been demonstrated that SiC MOSFETs are a viable option for high power density DC converters, capable of operating at high switching frequencies and with efficiencies well above 97 %. In addition, the estimations of the performance for the switching and conduction losses, efficiencies and temperatures showed a good agreement with the experimental results.

In this prototype, the switching frequency was limited by the increased semiconductor losses at the minimum battery voltage; however, the estimations suggest that if this minimum voltage is increased to 300 V, the SiC power modules under evaluation could transfer more than 50 kW with switching frequencies above 100 kHz, which would bring further reductions to the size and weight of the filtering and magnetic components. From the total weight of the converter, about 80 % was due to the magnetic devices and cooling hardware; therefore, this work also highlights the need for further research and development of magnetic materials, thermal materials and cooling techniques to reduce overall converter size.

The measured switching waveforms showed that, although being used in a hard-switched converter, SiC MOSFETs are one step towards the idealised power switch with instant switching times and lossless transitions; however, techniques are required to ameliorate the effects of stray inductance and the increasingly rapid rates of change of voltage and current.

## Acknowledgements

This work was undertaken as part of a collaborative research programme co-funded by the Technology Strategy Board under the Low Carbon Vehicle initiative. The authors gratefully acknowledge the financial support of the UK Technology Strategy Board and the technical contributions made by the project partners: Prodrive (project leader), Raytheon Systems Ltd. UK, IST Power Products, Tata Motors European Technical Centre, and SCISYS.

The authors are also grateful to Dr. Ian Hawkins for the design of the main PCB for the gate drivers.

## References

[1] J. Millan, P. Godignon, X. Perpina, A. Perez-Tomas, and J. Rebollo, "A Survey of Wide Bandgap Power Semiconductor Devices," *IEEE Transactions on Power Electronics,* vol. 29, pp. 2155-2163, May 2014.

[2] G. Calderon-Lopez, A. J. Forsyth, D. Gordon, and J. McIntosh, "Evaluation of SiC BJTs for High Power DC-DC Converters," *IEEE Transactions on Power Electronics,* vol. 29, pp. 2474-2481, May 2014.

[3] M. Hirakawa, M. Nagano, Y. Watanabe, K. Andoh, S. Nakatomi, and S. Hashino, "High Power Density DC/DC Converter using the Close-Coupled Inductors," in *IEEE Energy Conversion Congress and Exposition, ECCE*, 2009, pp. 1760-1767.

[4] M. Hirakawa, M. Nagano, Y. Watanabe, K. Ando, S. Nakatomi, S. Hashino, and T. Shimizu, "High Power Density Interleaved DC/DC Converter using a 3-phase Integrated Close-Coupled Inductor Set aimed for Electric Vehicles," *IEEE Energy Conversion Congress and Exposition, ECCE* 2010 pp. 2451-2457.

[5] G. Calderon-Lopez, A. J. Forsyth, and D. R. Nuttall, "Design and Performance Evaluation of a 10-kW Interleaved Boost Converter for a Fuel Cell Electric Vehicle," in *5th International Power Electronics and Motion Control Conference*, China, 2006, pp. 1328-1332.

[6] P. James, A. J. Forsyth, G. Calderon-Lopez, and V. Pickert, "DC-DC converter for hybrid and all electric vehicles," in *24th International Battery, Hybrid and Fuel Cell Electric Vehicle Symposium and Exhibition*, Norway, 2009, pp. 1-9.

[7] F. J. Bryan and A. J. Forsyth, "A Power Dense DC-DC Converter for a Small Electric Vehicle," in *6th International Conference on Power Electronics, Machines and Drives*, UK, 2012.

[8] CREE Inc., "CAS100H12AM1 1.2kV, 100A Silicon Carbide Half-Bridge Module" Product datasheet, Rev. B, USA, 2013.

[9] Hitachi Metals Ltd., "Metglas AMCC Series Cut Core/ Finemet F3CC Series Cut Core" Power Electronics Components [Catalog], Japan, 2010.

[10] Lytron Inc., "Standard & Custom Products", vol. 10, CP12 Press-Lock Cold Plates, pp. 13-30, USA, 2008.

[11] CT-Concept Technologie AG, "2SC0650P Description & Application Manual," CONCEPT, 2012. www.igbt-driver.com/go/2SC0650P.

[12] CT-Concept Technologie AG, "Application with SCALE-2 Gate Driver Cores," Application Note AN-1101, CONCEPT, 2011, http://igbt-driver.com/ support/application-notes.